Acta Pharmaceutica Sinica B 2021;11(12):3791−3805

Chinese Pharmaceutical Association
Institute of Materia Medica, Chinese Academy of Medical Sciences

Acta Pharmaceutica Sinica B

www.elsevier.com/locate/apsb
www.sciencedirect.com

ORIGINAL ARTICLE

Dual roles of p62/SQSTM1 in the injury and recovery phases of acetaminophen-induced liver injury in mice

Hui Qian[a,†], Qingyun Bai[a,b,c,†], Xiao Yang[a,b], Jephte Y. Akakpo[a], Lili Ji[b], Li Yang[b], Thomas Rülicke[d], Kurt Zatloukal[e], Hartmut Jaeschke[a], Hong-Min Ni[a], Wen-Xing Ding[a,*]

[a]*Department of Pharmacology, Toxicology and Therapeutics, University of Kansas Medical Center, Kansas City, KS 66160, USA*
[b]*The MOE Key Laboratory for Standardization of Chinese Medicines, Shanghai Key Laboratory of Compound Chinese Medicines and the SATCM Key Laboratory for New Resources and Quality Evaluation of Chinese Medicines, Institute of Chinese Materia Medica, Shanghai University of Traditional Chinese Medicine, Shanghai 201203, China*
[c]*School of Chemistry and Bioengineering, Yichun University, Yichun 336000, China*
[d]*Department of Biomedical Sciences, University of Veterinary Medicine Vienna Veterinärplatz, Vienna 1210, Austria*
[e]*The Institute of Pathology, Medical University of Graz, Graz A-8036, Austria*

Received 30 October 2021; received in revised form 5 November 2021; accepted 8 November 2021

KEY WORDS

Autophagy;
Coagulation;
DILI;

Abstract Acetaminophen (APAP) overdose can induce liver injury and is the most frequent cause of acute liver failure in the United States. We investigated the role of p62/SQSTM1 (referred to as p62) in APAP-induced liver injury (AILI) in mice. We found that the hepatic protein levels of p62 dramatically increased at 24 h after APAP treatment, which was inversely correlated with the hepatic levels of APAP-

Abbreviations: 4EBP-1, translational initiation factor 4E binding protein-1; AILI, APAP-induced liver injury; ALT, alanine aminotransferase; APAP, acetaminophen; APAP-AD, APAP-adducts; CLEC-2, C-type lectin-like receptor; CYP2E1, cytochrome P450 2E; GCL, glutamate cysteine ligase; GSH, glutathione; H&E, hematoxylin and eosin; KC, Kupffer cells; KEAP1, Kelch-like ECH-associated protein-1; KIR, KEAP1-interacting region; KO, knockout; LC3, microtubule-associated light chain 3; NAC, *N*-acetylcysteine; NAPQI, *N*-acetyl-*p*-benzoquinone imine; NF-κB, nuclear factor-κB; NPCs, non-parenchymal cells; NQO1, NADPH quinone dehydrogenase 1; NRF2, nuclear factor erythroid 2-related factor 2; S6, ribosomal protein S6 kinase; TUNEL, terminal deoxynucleotidyl transferase dUTP nick end labeling; VWF, von Willebrand factor; WT, wild type.

*Corresponding author. Tel.: +1 913 588 9813; fax: +1 913 588 7501.
E-mail address: wxding@kumc.edu (Wen-Xing Ding).
[†]These authors made equal contributions to this work.

Peer review under responsibility of Chinese Pharmaceutical Association and Institute of Materia Medica, Chinese Academy of Medical Sciences.

https://doi.org/10.1016/j.apsb.2021.11.010

Liver regeneration;
Macrophage;
Hepatotoxicity;
Platelet

adducts. APAP also activated mTOR at 24 h, which is associated with increased cell proliferation. In contrast, p62 knockout (KO) mice showed increased hepatic levels of APAP-adducts detected by a specific antibody using Western blot analysis but decreased mTOR activation and cell proliferation with aggravated liver injury at 24 h after APAP treatment. Surprisingly, p62 KO mice recovered from AILI whereas the wild-type mice still sustained liver injury at 48 h. We found increased number of infiltrated macrophages in p62 KO mice that were accompanied with decreased hepatic von Willebrand factor (VWF) and platelet aggregation, which are associated with increased cell proliferation and improved liver injury at 48 h after APAP treatment. Our data indicate that p62 inhibits the late injury phase of AILI by increasing autophagic selective removal of APAP-adducts and mitochondria but impairs the recovery phase of AILI likely by enhancing hepatic blood coagulation.

1. Introduction

Acetaminophen (APAP) is used primarily as an analgesic (pain relievers) and antipyretic (fever reduction) drug[1−3]. APAP overdose leads to severe hepatotoxicity, which attributes to nearly half of drug-induced liver injury and around 500 yearly deaths in Western countries[4−6]. Currently, the most commonly used treatment for APAP-induced liver injury (AILI) in clinic is *N*-acetylcysteine (NAC), which restores liver glutathione (GSH). However the time window for treatment with NAC is limited[7]. It is still necessary to develop novel treatments for APAP overdose. There are several distinctive phases of liver pathogenesis in AILI. In the early metabolic phase, APAP is oxidized by cytochrome P450 2E1 (CYP2E1) and CYP1A2 to generate highly reactive intermediate metabolite *N*-acetyl-*p*-benzoquinone imine (NAPQI), which is detoxified by hepatic GSH. However, excessive NAPQI can deplete both intracellular and mitochondrial GSH in hepatocytes, and the remaining NAPQI covalently binds to intracellular proteins and nucleic acids, resulting in the formation of APAP-adducts (APAP-AD). Some of the APAP-AD are formed on mitochondria that leads to mitochondrial damage and increased oxidative stress triggering hepatocyte necrosis and the necrotic injury phase[8−11]. Following the early metabolic and necrotic injury phase, several adaptive events occur in the liver including the innate immune response and blood coagulation events, which may either exacerbate or suppress AILI at the recovery phase[12−14]. Infiltrated macrophages from the blood circulation can help to resolve the injury by removing necrotic cells and induction of neutrophil apoptosis[15]. More recent evidence suggests that increased hepatic platelet aggregation as a result of increased secretion of the platelet-adhesive protein von Willebrand factor (VWF) in the liver inhibits liver regeneration in the late recovery phase of AILI[16].

We previously demonstrated that autophagy, a lysosomal degradation pathway, protects against AILI by promoting the removal of APAP-AD and damaged mitochondria[17−19]. p62/SQSTM1 (hereafter referred to as p62) is a multidomain scaffold protein and intracellular signaling hub for various signaling pathways[20−22]. p62 serves as an autophagy receptor protein for selective autophagy, which is primarily due to its direct interaction with the microtubule light chain 3 (LC3) protein that specifically localizes on autophagosome membranes[23]. We previously demonstrated that knockdown of p62 using adenovirus shRNA significantly increased APAP-AD in primary hepatocytes[17], suggesting that p62 may be involved in autophagic removal of APAP-AD. However, whether p62 is also required for autophagic removal of APAP-AD and plays a role in AILI *in vivo* are unknown.

In addition to serving as an autophagy receptor, p62 is involved in many intracellular signaling pathways. p62 directly interacts with Kelch-like ECH-associated protein 1 (KEAP1) though the KEAP1-interacting region (KIR) and activates nuclear factor erythroid 2-related factor 2 (*nfe2l2* or NRF2) in a noncanonical manner[24−26]. NRF2 activation induces gene expression of GSH synthesis and antioxidant as well as detoxify enzymes, such as glutamate cysteine ligase (GCL) and NADPH quinone dehydrogenase 1 (NQO1), to protect against AILI[27,28]. Liver-specific *Atg5* knockout (KO) mice have increased hepatic p62 accumulation resulting in NRF2 activation that leads to increased hepatic levels of NQO1, improved GSH recovery and attenuated AILI[29]. Moreover, p62 also regulates nuclear factor-κB (NF-κB) and mTORC1 activation[21,30,31], which may be involved in the liver regeneration phase from AILI. However, whether and how p62 would be involved in liver repair/regeneration phase following APAP overdose is unknown.

In the present study, we discovered complex dual roles of p62 in AILI in mice. p62 protected against the early phase of AILI likely by promoting the removal of APAP-AD and damaged mitochondria. However, p62 impaired late phase of liver repair/regeneration by increasing hepatic coagulation in AILI.

2. Materials and methods

2.1. Animal experiments

p62 knockout (KO) mice generated by Dr. Thomas Rülicke's laboratory and characterized in Kurt Zatloukal's laboratory, as described previously[32,33] and were back crossed to C57BL/6J background for more than 8 generations. Male and female $p62^{+/-}$ mice were then used as breed pairs to generate p62 wild type (WT) mice and p62 KO mice. All mice received human care, and all procedures were approved by the Institutional Animal Care and Use Committee of the University of Kansas Medical Center (Kansas City, KS, USA). Male matched wild-type and p62 KO mice at around 2−3 month-old were used for all experiments. Briefly, fed mice were treated with 500 mg/kg APAP (Sigma−Aldrich, A5000) dissolved in warm saline or saline alone *via* intraperitoneal injection. The blood and liver tissues were collected from mice that were euthanized

after APAP treatment for 6, 24 and 48 h. Liver injury was determined by serum alanine aminotransferase (ALT) kit from Pointe Scientific (T7526-450).

2.2. Histology and immunohistochemistry

Immunohistochemistry was performed as described previously[18]. Briefly, paraffin-embedded liver sections were stained by hematoxylin and eosin (H&E), and immunohistochemistry were employed with corresponding primary antibodies at 1:200 dilution overnight at 4 °C. After development with DAB (Vector Labs, Burlingame, CA, USA), the tissues were counterstained with hematoxylin (RICCA, 3530-32). Finally, the slides were covered with the mounting medium (Thermo Scientific, 8310-16) and observed under a Nikon microscope. Terminal deoxynucleotidyl transferase dUTP nick end labeling (TUNEL) staining was performed in paraffin-embedded liver sections using the *In Situ* Cell Death Detection TUNEL Kit from Roche (ROCHE-11684809910). Necrosis areas were estimated by scanning the entire tissue sections/slides from 3 to 9 mice in each group, and presented as the percentage of the total liver section areas.

2.3. Immunofluorescence staining and confocal microscopy

For the immunostaining assay, the procedures were followed as previously described[34]. Briefly, fresh liver tissues from APAP treated mice were fixed in 4% paraformaldehyde overnight at 4 °C and then transferred to 20% sucrose in PBS and stored at 4 °C for 24 h followed by mounting liver tissue in O.C.T. and stored at −80 °C. Five-micrometer sections were used for immunostaining. Liver tissue sections were immunostained with the anti-F4/80 (eBioscience, 14-4801-85), anti-VWF (Invitrogen, PA5-16634), anti-CD41 (BD Pharmingen, 553847), or anti-cleaved caspase-3 (Asp175; Cell Signaling, cs9661L) antibody followed by Alexa488 or red-conjugated secondary antibody. Confocal images were obtained using a Leica confocal microscope. The VWF positive areas, CD41 positive areas and number of F4/80 positive cells were analyzed using ImageJ (National Institutes of Health, Bethesda, MD, USA). Briefly, RGB images were converted into 8-bit images, and then a threshold of positive area was adjusted and set up. The positive areas of the images were then analyzed using Analyze > Set Measurements. For counting the number of F4/80 positive cells, Plugins > Analyze > Cell counter were chosen and total cell numbers were manually counted. At least 5 images from each mouse were quantified from four WT mice and five p62 KO mice with 24 h post APAP treatment.

2.4. Electron microscopy

For electron microscopy studies, fresh liver tissues were fixed in 2.5% glutaraldehyde in 0.1 mol/L phosphate buffer (pH 7.4), followed by 1% OsO_4. After dehydration, the tissues were cut into thin sections and stained uranyl acetate and lead citrate for observation under a JEM 1016CX electron microscope (JEOL, Tokyo, Japan). The number of autophagosomes that enveloped with mitochondria (mitophagosomes) was counted and normalized to the cytosolic areas using a SPOT software (SPOT Imaging).

2.5. Western blot analysis

Small pieces of mouse liver were homogenized by three times of 10 s sonication in RIPA buffer [1% NP40, 0.5% sodium deoxycholate, 0.1% sodium dodecyl (lauryl) sulfate] with freshly added proteinase inhibitor. The protein concentrations were quantified using BCA (Pierce Protein Reagent Assay BCA Kit, 23228). Total liver lysate (30 μg/well) from each sample was separated by SDS-PAGE and transferred to PVDF membranes, and blocked with 5% non-fat milk in TBST at room temperature for 1 h with shaking. Membranes were probed with various primary and secondary antibodies, and the protein bands were developed with SuperSignal West Pico chemiluminescent substrate (Thermo Scientific, 34578). The following antibodies were used for Western blot analysis: 4E-BP1 (Cell Signaling, cs9452), phosphor-4E-BP1 (Ser65) (Cell Signaling, cs9451), CYP2E1 (Abcam, Ab789013), cyclin D1(Santa Cruz, sc-450), CD41 (BD Pharmingen, 553847), phosphor-JNK (Cell Signaling, cs9255), total-JNK (Cell Signaling, cs9252), LC3B (Cell Signaling, cs3868), OXPHOS cocktail (Abcam, Ab110413), p62/SQSTM1 (Abnova, H00008878-M01), PCNA (Santa Cruz, sc-56), S6 (Cell Signaling, cs2217), phosphor-S6 (Cell Signaling, cs4858), VWF (Invitrogen, PA5-16634), and β-actin (Sigma−Aldrich, a5541). GCLC and GCLM antibodies were gifts from Dr. Terry Kavanagh (University of Washington, Seattle, WA, USA). The APAP-adduct antibody was a gift from Dr. Lance Pohl (NIH, USA). The results were analyzed by ImageJ (National Institutes of Health, Bethesda, MD, USA).

2.6. RNA extraction and real-time polymerase chain reaction (PCR)

RNA was isolated from liver tissue with TRIzol Reagent (Invitrogen) according to the manufacturer's instructions. RNA concentration and quality were determined by spectrophotometer, and the complementary DNA was prepared as described[29]. Real-time PCR was used to determine mRNA levels of target genes using a Bio-Rad CFX384 Touch Real-Time PCR Detection System with Maxima SYBR green/rox qPCR reagents (Bimake, B21202). β-Actin or 18S were used for normalization. The following sequences of primers were used for mRNA level detection: *Atg8* forward, 5′-CCGAGAAGACCTTCAAGCAG-3′, and *Atg8* reverse, 5′-ACAC TTCGGAGATGGGAGTG-3′; cyclin D1 (*Ccnd1*) forward, 5′-GC CATCCAAACTGAGGAAAA-3′, and cyclin D1 (*Ccnd1*) reverse, 5′-GATCCTGGGAGTCATCGGTA-3′; *Gclc* forward, 5′-AACACA-GACCCAACCCAGAG-3′, and *Gclc* reverse, 5′-CCGC ATCTTCTGGAAATGTT-3′; *Gclm* forward, 5′-TGTGTGATGC-CACCAGATTT-3′, and *Gclm* reverse, 5′-GATGATTCCC CTGCTCTTCA-3′; *Nqo1* forward, 5′-CAGATCCTGGAAGGAT GGAA-3′, and *Nqo1* reverse, 5′-TCTGGTTGTCAGCTGGAATG-3′; p62/*Sqstm1* forward, 5′-AGAATGTGGGGGAGAGTGTG-3′, and p62/*Sqstm1* reverse, 5′-TCGTCTCCTCCTGAGCAGTT-3′; β-actin forward, 5′-TGTTACCAACTGGGACGACA-3′, and β-actin reverse, 5′-GGGGTGTTGAAGGTCTCAAA-3′; 18S forward, 5′-GAGCGAAAGCATTTGCCAAG-3′, and 18S reverse, 5′-GGCATCGTTTATGGTCGGAA-3′.

2.7. Glutathione (GSH) assay and APAP-adducts detection

Hepatic GSH levels in mouse livers were measured using a modified Tietze assay with modifications as described[35]. Briefly, liver tissue was homogenized in sulfosalicylic acid (3%) followed by centrifugation, and the collected supernatant was further

diluted in potassium phosphate buffer. The sample was then assayed using glutathione reductase dithionitrobenzoic acid, and GSH levels were determined by spectrophotometry at 412 nm[19]. Liver APAP-cysteine (APAP-Cys) adducts were quantified by high pressure liquid chromatography (HPLC) with electrochemical detection (ED) as described previously[29,36].

2.8. *Serum VWF quantification by enzyme-linked immunoassay (ELISA)*

Serum samples were collected as described above. The serum VWF levels were measured using a Mouse Von Willebrand Factor A2 ELISA Kit (Abcam, ab208980), following the manufacturer's instructions. Briefly, 2 μL serum was added into 298 μL sample diluent from the kit. Fifty μL diluted samples and 50 μL of the Antibody Cocktail were loaded into each well, respectively. The plate was sealed and incubated for 1 h at room temperature on a plate shaker and then washed with washing buffer for 4−6 times. After the last wash, 100 μL substrate solution was added into each well, after which it was incubated for 10 min in the dark on a plate shaker. And then 100 μL stop solution was loaded into each well and the well was mixed on plate shaker for 1 min. The absorbance at 450 nm was recorded and used for serum VWF quantification.

2.9. *Statistical analysis*

Data were analyzed by Student *t*-test, one-way analysis of variance (ANOVA) with Tukey's HSD *post hoc* test or Dunnett's *post hoc* test to evaluate the statistical differences by R[37] and R studio[38] when appropriate. The value of P critical value $\leq P$ ($\alpha = 0.05$) was considered statistically significant among groups. All experiments data were reported as mean ± standard error (SE).

3. Results

3.1. *p62 KO mice are more susceptible to AILI in the early injury phase*

To determine whether APAP would affect the hepatic levels of p62, we treated WT mice with 500 mg/kg APAP for 6 and 24 h. Immunoblot analysis showed that the hepatic levels of p62 did not change at 6 h but dramatically increased at 24 h after APAP treatment. Hepatic levels of LC3-II, which reflects the number of autophagosomes, also increased at 24 h after APAP treatment (Fig. 1A). Immunohistochemistry staining for p62 also confirmed increased p62 staining in hepatocytes mainly close to the central lobular necrotic areas in APAP-treated mouse livers (Fig. 1B, arrows), which we named as zone 2 hepatocytes (Fig. 1C). p62 is an autophagy substrate protein and increased autophagy often leads to p62 degradation. To determine whether increased p62 at 24 h after APAP treatment could also be regulated at the transcription level in addition to autophagic degradation, we performed qRT-PCR analysis using mRNA extracted from these mouse livers. We found that the mRNA levels of *p62/Sqstm1* and *Atg8/LC3B* significantly increased at 6 h after APAP treatment but returned almost to the same levels of the control mice at 24 h after APAP (Fig. 1D).

To determine whether increased hepatic p62 protects against APAP-induced liver injury, we treated both WT and p62 KO mice

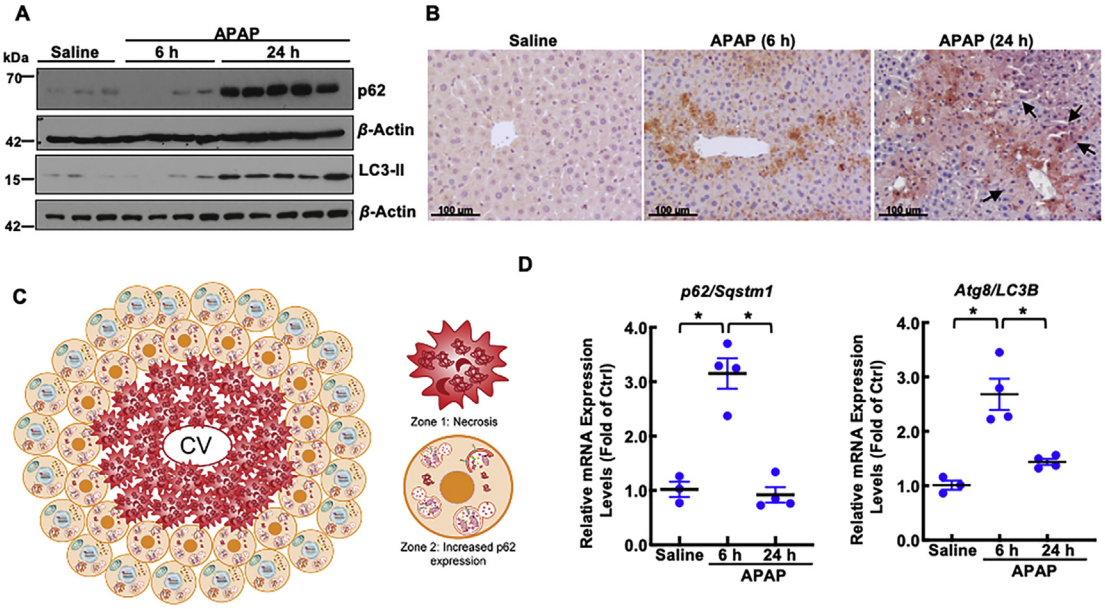

Figure 1 Hepatic protein levels of p62/SQSTM1 increased at 24 h but not at 6 h after APAP treatment. Male wild-type (WT) and p62-knockout (KO) mice were treated with APAP (500 mg/kg, i.p.) or saline for 6 or 24 h. (A) Western blot analysis of p62 and LC3B from the total liver lysates. β-Actin is used as an internal control. (B) Representative images of immunohistochemical staining of liver p62 of wild-type mouse livers with different treatments. (C) An illustration of different levels of p62 protein expression in different zonations detected by IHC in APAP-induced mouse liver. Zone 1, necrotic cells in the central vein area; Zone 2, hepatocytes with high p62 expression adjacent the necrotic area. (D) qPCR analysis of mRNA from mouse livers. Results are normalized to β-actin and expressed as fold change compared to the control (Ctrl) group. Data shown are mean ± SE ($n \geq 3$). *$P < 0.05$ from one-way ANOVA followed by Tukey's HSD *post hoc* test.

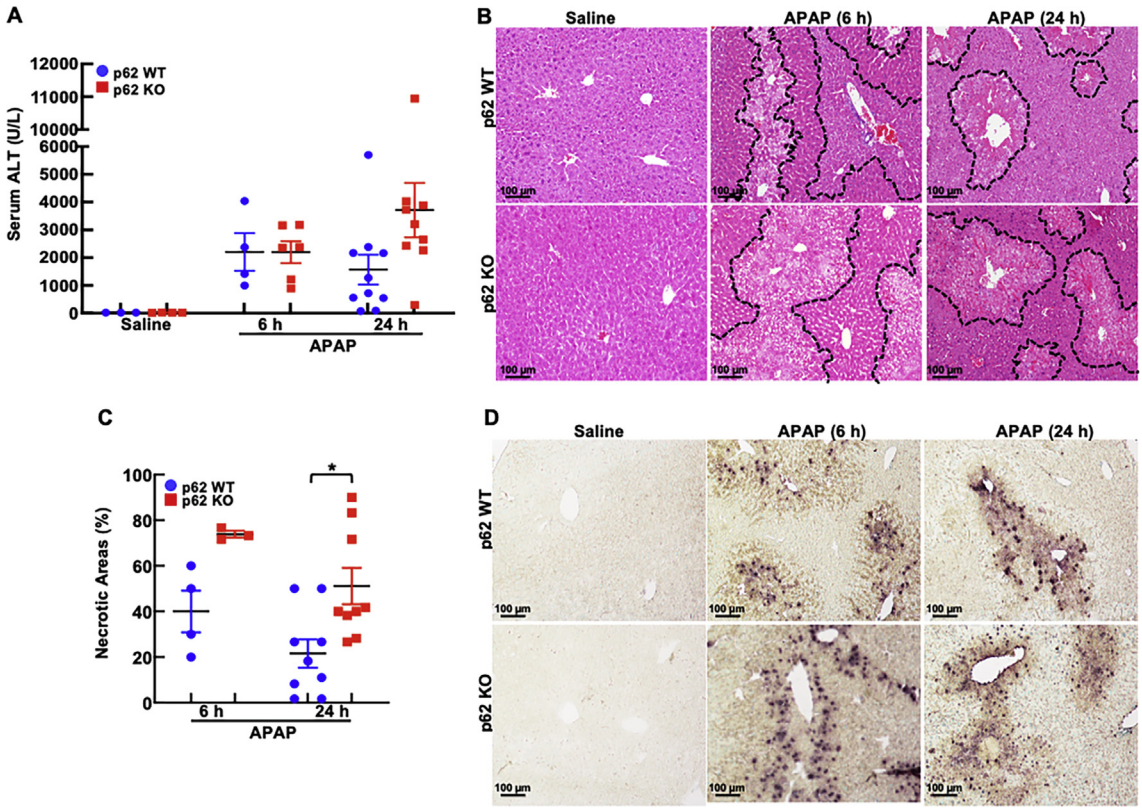

Figure 2 APAP induced more severe liver injury in p62 KO mice. Male WT and p62 KO mice were treated with APAP (500 mg/kg, i.p.) or saline for 6 or 24 h. (A) Level of serum ALT were quantified. Each dot represents one mouse, and data are presented as mean ± SE ($n \geq 3$) and analyzed by one-way ANOVA followed by Tukey's HSD *post hoc* test. (B) Representative images of H&E staining of mouse livers (magnification 100 ×). (C) Quantification of the necrotic areas from H&E staining of (B). Data are presented as mean ± SE ($n > 3$). *$P < 0.05$ from one-way ANOVA followed by Tukey's HSD *post hoc* test. (D) Representative images of TUNEL staining in mouse livers (magnification 100 ×).

with APAP (i.p., 500 mg/kg). We found that the serum levels of ALT markedly increased in both WT and p62 KO mice after APAP treatment for 6 h compared with the saline treated groups, and no significant differences were found between WT and KO mice. However, the serum levels of ALT were two-fold higher in p62 KO mice than in WT mice after APAP treatment for 24 h (Fig. 2A). Liver H&E and TUNEL staining showed increased necrosis areas accompanied with hemorrhage around the central lobular areas after APAP treatment in both WT and p62 KO mice (Fig. 2B−D). Consistent with the serum ALT data, necrotic areas were significantly higher in p62 KO mice than in WT mice at 24 h but not 6 h after APAP treatment (Fig. 2B−D). These results indicate that p62 KO mice are more susceptible to AILI in the late injury phase.

3.2. Delayed clearance of a subset group of hepatic and serum of APAP-AD and impaired GSH recovery in p62 KO mice

We found no significant difference in the hepatic levels of CYP2E1 between WT and p62 KO mice with or without APAP treatment (Fig. 3A and B). Using an antibody that is specific for APAP-AD, we found that the levels of hepatic and serum APAP-AD were much higher in p62 KO mice than in WT mice after APAP treatment at either 6 or 24 h (Fig. 3A−F). In WT mice, the levels of APAP-AD were higher at 6 h but declined at 24 h after APAP treatment in both liver (Fig. 3C) and serum (Fig. 3F). However, the levels of APAP-AD sustained from 6 to 24 h after APAP treatment in p62 KO mice (Fig. 3C and F). As APAP-AD antibody may only recognize a portion of but not all APAP-AD in the mouse livers, we next quantified hepatic APAP-AD using the HPLC analysis. Interestingly, consistent with the Western blot analysis results, we observed a time-dependent decrease of hepatic APAP-AD post APAP treatment in both WT and p62 KO mice. However, no differences for the levels of APAP-AD were found between WT and p62 KO mice (Fig. 3G), suggesting that p62 may only be required for the clearance of a subset group of specific (proteins mainly around 38 and 52 kDa) but not all APAP-AD in mouse livers.

The early phase of bioactivation of APAP can lead to the depletion of hepatic GSH. Indeed, we found that the levels of hepatic GSH decreased markedly at 2 h after APAP treatment in both WT and p62 KO mice, suggesting that the bioactivation and metabolism of APAP are not altered in p62 KO mice. The levels of hepatic GSH started to recover at 6 h and returned to the basal levels at 24 h after APAP treatment in WT mice. In contrast, while the levels of hepatic GSH also started to recover at 6 h and further increased at 24 h after APAP treatment in p62 KO mice, the levels of GSH were significantly lower in p62 KO mice than in WT mice (Fig. 4A), suggesting lack of p62 delayed the recovery of hepatic GSH after APAP overdose.

Glutamate cysteine ligase (GCL) is the rate-limiting enzyme for the synthesis of cellular GSH. GCL is composed of catalytic (GCLC) and modifier (GCLM) subunits, which are regulated at the transcription level by NRF2. p62, in particular, phosphorylated p62 can bind to KEAP1 resulting in NRF2 activation[39]. In

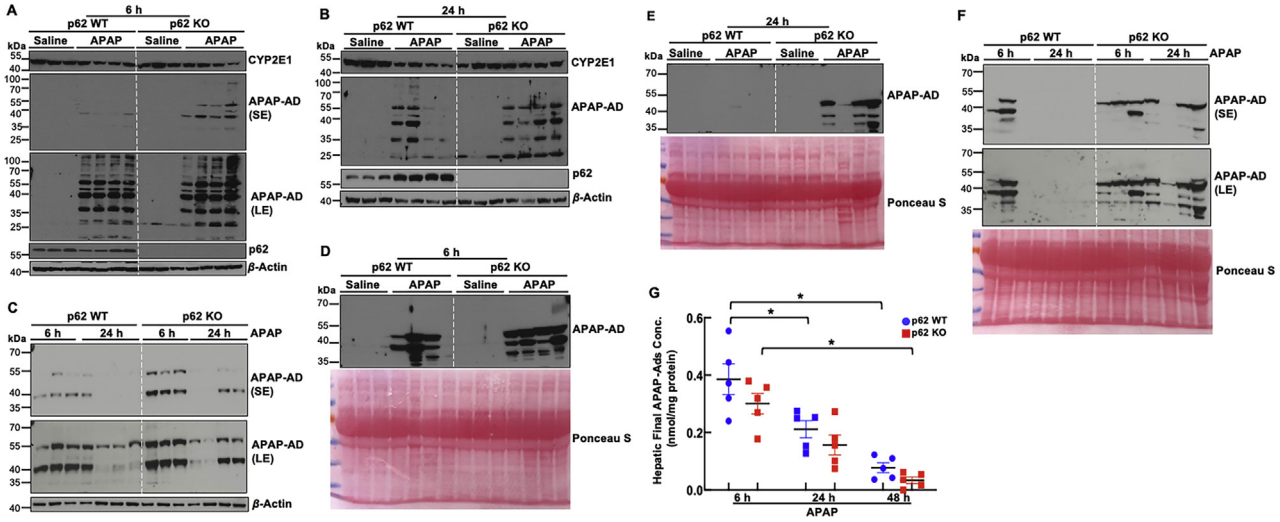

Figure 3 p62 KO mice have increased levels of a subset group of APAP-adducts. Male WT and p62 KO mice were treated with APAP (500 mg/kg, i.p.) or saline for 6 or 24 h. (A−C) Western blot analysis of CYP2E1 and APAP-AD from total liver lysates. β-Actin was used as an internal control. (D−F) Western analysis of serum samples from WT and p62 KO mice that were treated with APAP (500 mg/kg, i.p.) for 6 or 24 h. Ponceau S red staining of the membrane serves as a loading control. LE, longer exposure; SE, shorter exposure. (G) Liver samples collected 6 and 24 h post-APAP and were analyzed for APAP-AD, and data are presented as means ± SE ($n = 3-5$). *$P < 0.05$, one-way ANOVA followed by Tukey's HSD *post hoc* test.

addition to total p62, we found that the levels of phosphorylated p62 also increased at 24 h after APAP treatment in WT mice. Interestingly, the levels of GCLC and GCLM also increased at 24 h after APAP treatment in WT mice, which were significantly higher than p62 KO mice (Fig. 4B and C). Consistent with the protein changes, we found that the mRNA levels of *Gclc* in WT mice were higher than in p62 KO mice at 24 h after APAP treatment. The mRNA levels of *Gclm* and *Nqo1* were also significantly higher in WT mice than in p62 KO mice at 24 h after APAP treatment (Fig. 4D). Together, these results indicate that p62 KO mice do not affect the metabolic activation of APAP but have reduced ability to remove specific APAP-adduct and impaired hepatic GSH recovery likely due to impaired NRF2 activation.

3.3. *Impaired mitophagy in APAP-treated p62 KO mice*

APAP exposure can activate hepatic JNK and mitochondrial translocation that aggravates mitochondrial damage and mitochondrial oxidative stress, which promotes AILI[40,41]. We found that the levels of phosphorylated JNK markedly increased at 6 h but returned to undetectable baseline levels at 24 h after APAP treatment in both WT and p62 KO mice (Fig. 5A), suggesting the exacerbated AILI in p62 KO mice is independent of JNK activation.

We previously showed that autophagic removal of damaged mitochondria protects against AILI[18,19]. Mitophagy is a selective process that is mediated by several mitophagy receptor proteins including p62[42−44]. We next determined whether lack of p62 would affect mitophagy after APAP overdose. Degradation of inner mitochondrial membrane proteins is generally a reliable marker for mitophagy. We found that the hepatic levels of several inner mitochondrial membrane proteins of oxidative phosphorylation proteins (consist of complexes I, II, III, IV and V) except complex I were generally higher in p62 KO mice than in WT mice at 24 h after APAP treatment (Fig. 5B and C), suggesting possible impaired mitophagy in p62 KO mice after APAP treatment. It should be noted that the hepatic levels of complexes V, III and IV in saline treated p62 KO mice were lower than WT mice. To further determine hepatic mitophagy, we performed electron microscopy studies and quantified the number of autophagosomes/autolysosomes that enwrapped with mitochondria. Mitophagy are referred to typical double membrane autophagosomes that enwrapped with mitochondria (Fig. 5D, arrows), which were readily detected in APAP-treated WT mouse livers. The number of autophagosomes that enwrapped with mitochondria was significantly lower in p62 KO mice than in WT mice after APAP treatment (Fig. 5E). These data indicate that p62 KO mice have impaired mitophagy in the injury phase of AILI.

3.4. *Lack of p62 decreases mTOR activation and impairs hepatocyte proliferation in the early recovery phase of AILI*

Since p62 interacts with Raptor, RagC and TRAF6 leading to the activation of mTORC1[22], we next determined whether lacking p62 would affect mTOR activity after APAP treatment in mouse liver. We found that the hepatic levels of phosphorylated 4EBP-1 and S6, two substrate proteins that are known to be phosphorylated by mTORC1, markedly increased in WT mice at 24 h after APAP treatment, which were blunted in p62 KO mice (Fig. 6A and B). IHC staining of liver tissues confirmed increased hepatic phosphorylated S6 protein, which are adjacent to the necrotic areas at 24 h after APAP treatment in WT mice but were decreased in p62 KO mice (Fig. 6C).

PCNA is a marker for cell proliferation. We found that the number of PCNA positive hepatocytes and non-parenchymal cells (NPCs) significantly increased in WT mice at 24 h after APAP-treatment, which were markedly blunted in p62 KO mice (Fig. 7A and B). Results from the immunoblot analysis also revealed increased hepatic levels of cyclin D1 and PCNA but decreased p21 in WT mice at 24 h after APAP treatment compared with the saline control groups. In contrast, the levels of cyclin D1 and PCNA were barely changed whereas the levels of p21 increased in p62 KO mice

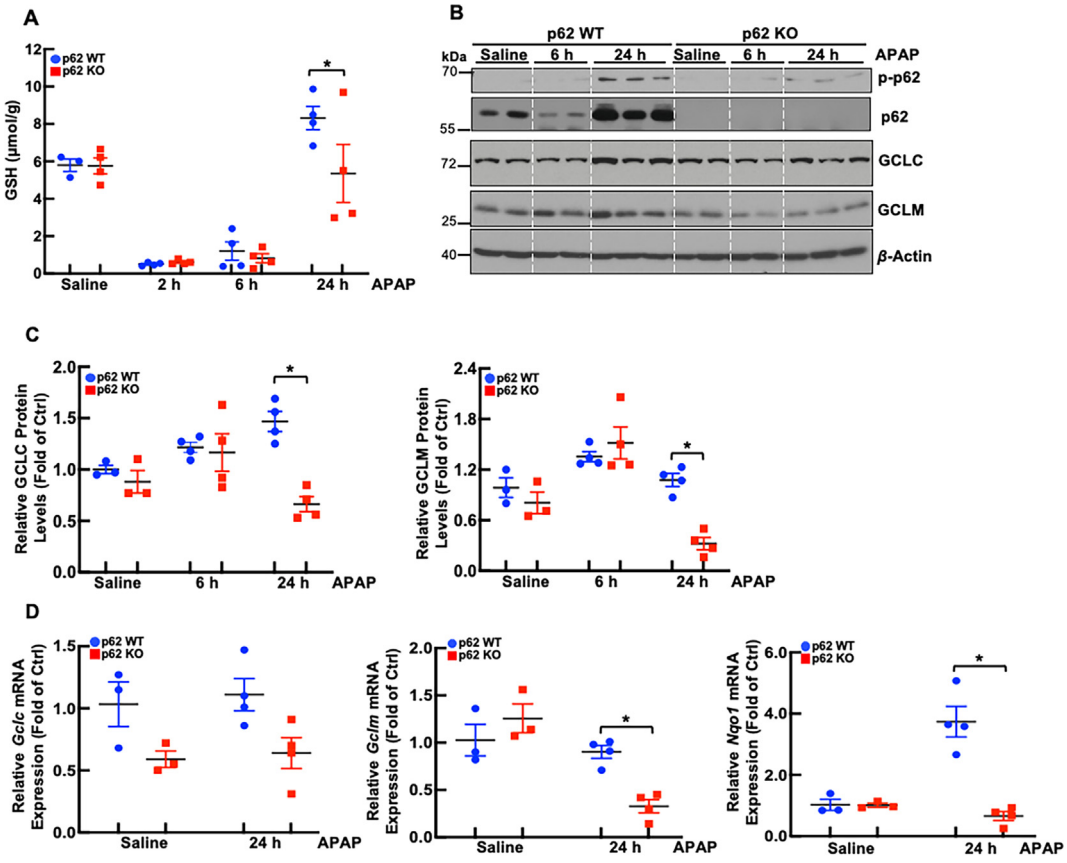

Figure 4 Decreased NRF2 activation in p62 KO mice after APAP treatment. Male WT and p62 KO mice were treated with APAP (500 mg/kg, i.p.) or saline for 2, 6 or 24 h. (A) Total hepatic GSH contents were determined, and data are presented as mean ± SE ($n = 3-5$). *$P < 0.05$, one-way ANOVA followed by Dunnett's *post hoc* test. (B) Western blot analysis of phosphorylated-p62 (p-p62), p62, GCLC, and GCLM of total liver lysates. β-Actin used as an internal control. (C) Densitometry analysis of GCLC and GCLM from the Western blot analysis. Data are presented as mean ± SEM ($n \geq 3$); *$P < 0.05$ from one-way ANOVA followed by Tukey's HSD *post hoc* test. (D) Quantitative real-time PCR analysis of the expression of *Gclc*, *Gclm* and *Nqo1* in mouse livers. Total RNAs were prepared from livers of the indicated genotypes. Data are presented as mean ± SEM ($n \geq 3$). *$P < 0.05$ from one-way ANOVA followed by Tukey's HSD *post hoc* test.

after APAP treatment compared with either the saline-treated p62 KO mice or WT mice (Fig. 7C). Moreover, we found that the hepatic mRNA levels of Cyclin D1 were almost 4-fold higher in WT mice liver compared with p62 KO mice at 24 h after APAP treatment (Fig. 7D). To further determine whether the expression levels of p62 would be correlated with the levels of PCNA after APAP treatment, we performed densitometry analysis for hepatic levels of PCNA and p62. We found a significant correlation between the levels of hepatic expression of PCNA and p62 ($R^2 = 0.5342$; $P = 0.003$) in livers of WT mice after APAP treatment (Fig. 7E and F). Taken together, these data suggest that p62 plays an important role in the early phase of liver repair/regeneration after APAP overdose likely by promoting mTORC1 activation in mice.

3.5. *p62 inhibits the late recovery phase of AILI by promoting hepatic VWF and platelet aggregation*

To investigate the role of p62 in the recovery phase of AILI, p62 KO and matched WT mice were treated with APAP for up to 48 h. Surprisingly, while WT mice still sustained high levels of serum ALT, the levels of ALT were dramatically decreased in p62 KO mice (Fig. 8A). Liver H&E and TUNEL staining also showed p62 KO mice had decreased hemorrhage and necrotic areas compared to WT mice, which is consistent with the lower levels of serum ALT (Fig. 8B and C). Interestingly, the number of PCNA positive NPCs but not hepatocytes markedly increased in p62 KO mice in comparison with WT mice (Fig. 8B and D). In addition, we also found the hepatic levels of GSH were completely recovered in p62 KO mouse livers and were not different from WT mice at 48 h after APAP treatment (Fig. 8E).

Accumulating evidence has implicated hepatic macrophages, VWF and platelet aggregation in the recovery phase of AILI[16,45–47]. Results from the IHC staining of F4/80 in liver tissues revealed no difference for the number of F4/80 positive macrophages/Kupffer cells between WT and p62 KO mice at 24 h after APAP treatment. However, the number of macrophages/Kupffer cells significantly increased in p62 KO mice than in WT mice at 48 h after APAP treatment (Fig. 9A and B). Consistent with IHC staining data, the hepatic mRNA levels of *F4/80* were 3-fold higher in p62 KO mice than in WT mice at 48 h after APAP treatment (Fig. 9C). Double immunostaining of cleaved caspase-3 and F4/80 revealed increased caspase-3 activation in p62 KO F4/80 positive cells in comparison with WT F4/80 positive cells (Fig. 9D and E), suggesting p62 deficiency may promote caspase activation and macrophage cell death in p62 KO mice post APAP treatment. Results from the immunofluorescence staining of VWF, CD41 and F4/80 revealed increased hepatic VWF and CD41 staining at 24 and 48 h after APAP treatment in

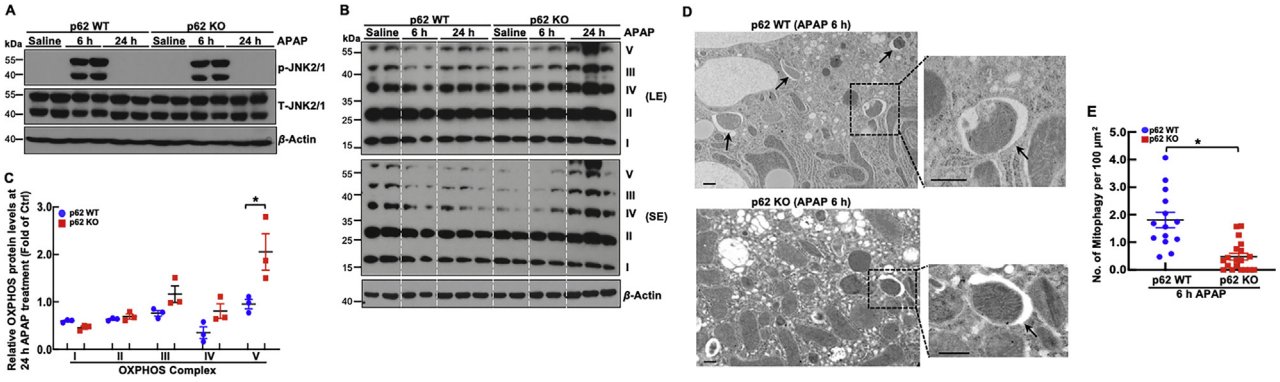

Figure 5 Decreased mitophagy in p62 KO mice after APAP treatment. Male wild type and p62 KO mice were treated with APAP (500 mg/kg, i.p.) or saline for 6 or 24 h. (A) Total liver lysates were subjected to Western blot analysis for phosphorylated-JNK and total-JNK. β-Actin is used as internal control. (B) Total liver lysates were subjected to Western blot analysis for mitochondrial oxidative phosphorylation (OXPHOS) proteins. (C) Densitometry analysis of (B). Data are presented as mean ± SEM ($n \geq 3$). *$P < 0.05$ from one-way ANOVA followed by Tukey's HSD *post hoc* test. (D) Representative EM images from WT and p62 KO mouse livers at 6 h after APAP treatment. Arrows denote mitophagy. Scale bar = 500 nm. (E) Quantification of the number of autophagosomes that enwrapped with mitochondria from EM. Data shown are mean ± SE (at least 10 images quantified per mouse). *$P < 0.05$ from Student *t*-test.

WT mice, which were markedly decreased in p62 KO mice at 48 h after APAP treatment (Fig. 10A−D), suggesting possible increased hepatic platelet aggregation and blood coagulation in APAP-treated WT mice. Interestingly, we observed increased co-localization of F4/80 and VWF signals (arrows in Fig. 10B enlarged lower panel), suggesting that it is possible that hepatic macrophage may help to remove excess hepatic VWF in APAP-treated mouse livers. Serum levels of VWF also increased in a time-dependent manner after APAP treatment although there was no significant difference between WT and p62 KO mice (Fig. 10E). Platelets (Fig. 10F, white arrows) and red blood cells (RBC) were also readily detected in the liver tissues by electron microscopy studies. We also found increased fibrin deposition in APAP-treated mouse livers (Fig. 10F, red arrow). Taken together, these data indicate that p62 deficiency promotes recovery from AILI likely by attenuating hepatic accumulation of VWF and platelet aggregations.

4. Discussion

In the present study, we found different role of p62 during the time-course of AILI in that p62 KO mice had increased liver injury compared with WT mice at 24 h after APAP treatment. Increased liver injury in p62 KO mice was associated with increased hepatic levels of a subset group of APAP-AD and decreased mTOR activation as well as decreased number of PCNA-positive hepatocytes. Paradoxically, while liver injury sustained in some WT mice at 48 h after APAP treatment, liver injury was markedly improved in all p62 KO mice that was associated with decreased hepatic VWF and platelet aggregation. These results indicate that p62 plays unique dual roles in AILI. In the early phase of AILI, p62 protects the liver against AILI by autophagic removal of specific APAP-AD and damaged mitochondria. However, in the late phase of AILI, p62 impairs the recovery from AILI by enhancing hepatic blood coagulation.

The multidomain protein p62 has multiple functions in cells, which may account for its complex dual roles in AILI[21,30,48]. As an autophagy receptor, p62 has a ubiquitin associated domain (UBA) at its C-terminus and LIR, which can bind to ubiquitinated cargos and autophagosome membrane, respectively. We have previously reported that autophagy can help to remove APAP-AD and damaged mitochondria and protect against the early phase of AILI[17−19]. APAP-AD are presented in the detergent insoluble fractions and mitochondria are ubiquitinated by parkin-dependent and independent mechanisms, and thus both APAP-AD and ubiquitinated mitochondria can bind with p62 and be recruited to autophagosomes for degradation[17,19]. In the present study, we further found that p62 does not affect the total hepatic levels of APAP-AD but may mainly selectively remove a subset group of specific APAP-AD around 38 and 52 kDa. It has been demonstrated that mitochondrial APAP-AD is more critical to promote mitochondrial damage and subsequent necrosis induced by APAP[49,50]. Future work is needed to further identify the nature of these 38 and 52 kDa APAP-AD, and whether they are exclusively on the mitochondria. Notably, the hepatic levels of complexes V, III and IV in saline treated p62 KO mice were lower than WT mice. Whether the decreased baseline levels of mitochondrial respiratory chain protein may also sensitive p62 KO mice to APAP hepatotoxicity needs to be investigated in the future by directly measuring the mitochondrial functions. Taken together, it is likely that impaired removal of a subset of specific APAP-AD and damaged mitochondria in p62 KO mice may contribute to the aggravated liver injury in the early phase of AILI.

In addition to serving as an autophagy receptor, p62 promotes the non-canonical NRF2 activation by interacting with KEAP1 *via* its KIR domain[20,22]. NRF2 activation can increase gene expression of hepatoxic detoxify enzymes, antioxidant and GSH synthesis genes, which protects against AILI[29,51]. We found markedly increased hepatic levels of p62 at 24 h after APAP treatment, which is correlated with increased NRF2 target gene expression and hepatic GSH recovery. In contrast, p62 KO mice had decreased NRF2 activation and delayed hepatic GSH recovery after APAP exposure. Accumulating evidence implicates JNK activation in AILI (Ramachandran and Jaeschke, 2018). A recent study reported that JNK can phosphorylate and inactivate NRF2 resulting in deceased expression of hepatic antioxidant genes[51]. However, these appear to be late effects, which are unlikely affecting the injury (Jaeschke and Ramachandran, 2021). Consistent with this interpretation, our data show that the phosphorylated levels of JNK were not different

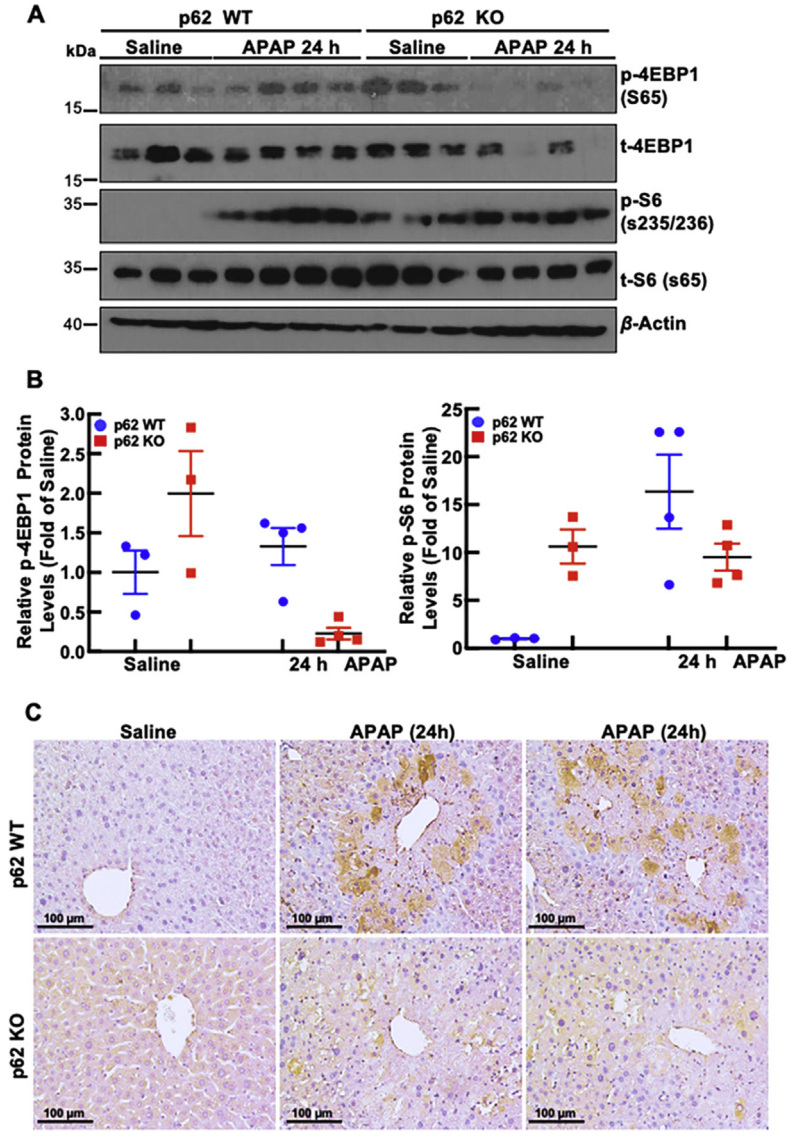

Figure 6 Decreased mTOR activation in p62 KO mice after APAP treatment. Male WT and P62 KO mice were treated with APAP (500 mg/kg, i.p.) or saline for 24 h. (A) Western blot analysis of S6, p-S6, 4EBP1, and p-4EBP1 of total liver lysates. (B) Densitometry analysis of p-S6 and p-4EBP1 from (A). Data are presented as mean ± SEM ($n \geq 3$). (C) Representative images of the immunohistochemical staining of the liver p-S6 in the indicated mice (magnification 200×).

among WT and p62 KO mice after APAP treatment. Therefore, it is likely that decreased NRF2 activation in p62 KO mice was mainly mediated *via* the non-canonical NRF2 pathway independent of JNK.

p62 also interacts with Raptor, RagC and TRAF6 to promote mTORC1 activation in an amino acid-dependent manner[20,22]. It has been reported that mTOR mediates liver regeneration after severe liver injury by regulating the dedifferentiation of biliary epithelial cells and the proliferation of bipotential progenitor cells-derived hepatocytes[52]. We found that the hepatic protein levels of p-S6 and p-4EBP1 increased at 24 h after APAP treatment, which positively correlated with increased number of PCNA-positive cells and hepatic p62 levels. In contrast, p62 KO mice showed decreased mTORC1 activation and reduced number of PCNA-positive cells at 24 h after APAP treatment. We previously showed that pharmacological inhibition of mTORC1 activates autophagy and protects against the early phase of AILI[53]. However, our more recent study showed that mice with liver-specific deletion of either Raptor or mTOR did not protect against AILI[54]. Therefore, the role of mTORC1 in AILI is complex and may be context-dependent. It is likely that in the early initiation phase of AILI, inhibition of mTOR may act primarily for the removal of APAP-AD and damaged mitochondria by activating autophagy. However, in the recovery phase of AILI, inhibition of mTOR may mainly inhibit cell proliferation and liver regeneration resulting in delayed liver recovery of AILI. Notably, paradoxical role of mTOR in either inhibiting or promoting liver tumorigenesis in mice has also been reported[55,56]. Therefore, the role of mTOR and autophagy in AILI is complex and more future studies are needed to further elucidate their roles in AILI and other types of liver injury.

Increasing evidence have implicated inflammation and blood coagulation in AILI[14,47,57,58]. Following the extensive necrosis

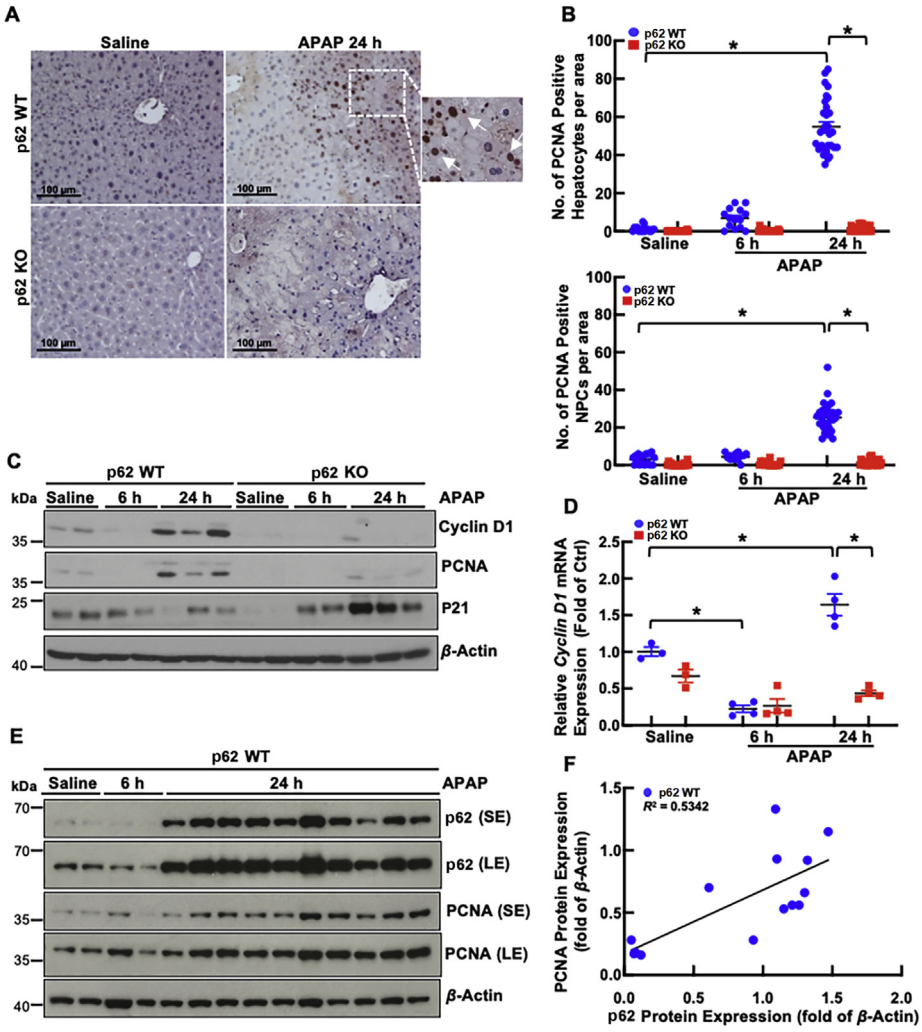

Figure 7 Impaired liver regeneration in p62 KO mice after APAP-treatment in the early injury phase. Male WT and p62 KO mice were treated with APAP (500 mg/kg, i.p.) or saline for 24 h. (A) Representative images of immunohistochemical staining of PCNA in mouse livers (magnification 200×). (B) Quantification of the PCNA-positive hepatocytes and PCNA-positive non-parenchymal cells (NPCs) of (A). Data are presented as mean ± SE ($n > 10$). *$P < 0.05$ from one-way ANOVA followed by Tukey's HSD *post hoc* test. (C) Western blot analysis of PCNA, cyclin D and p21 in total liver lysates. β-Actin is used as internal control. (D) Quantitative real-time PCR analysis of the expression of cyclin D1 in mouse livers. Data are presented as mean ± SEM ($n = 4$). *$P < 0.05$ from one-way ANOVA followed by Tukey's HSD *post hoc* test. (E) Western blot analysis of p62 and PCNA in total liver lysates of WT mice. β-Actin is used as internal control. (F) A scatter plot and linear regression analysis of expression levels of PCNA *vs*. p62 in WT mice treated with APAP for 24 h. LE, longer exposure; SE, shorter exposure.

induced by APAP, several damage-associated molecular patterns (DAMPs) including nuclear and mitochondrial DNA as well as the nuclear high-mobility group box 1 protein are released from the hepatocytes, which trigger the sterile inflammation. Activated Kupffer cells/macrophages by the DAMPs produce various cytokines including TNF-α and interleukin-1β as well as other chemokines, which further recruit circulating monocyte-derived macrophages and neutrophils in the liver.

We found increased F4/80 positive cells in the areas adjacent to necrotic cells in p62 KO mice 48 h post APAP treatment, which are most likely derived from the circulating monocytes that help to clear the debris of necrotic hepatocytes. Paradoxically, we found increased caspase-3 activation in p62 KO Kupffer cells although the number of F4/80 positive cells was not different among WT and p62 KO mice 24 h post APAP treatment. It remains unclear why the number of F4/80 positive KC/macrophages increased in p62 KO mice 48 h post APAP treatment. It is likely that p62 KO mice may have increased infiltrated monocytes from the circulation 48 h post APAP treatment than WT mice. Future studies are needed to further investigate the nature of these F4/80 positive cells post APAP treatment in p62 KO mice. Completely elimination of KC population using clodronate-loaded liposomes aggravates liver injury whereas partial elimination of KC by pretreatment with gadolinium chloride ($GdCl_3$) attenuates liver injury[45,59]. Ethyl pyruvate (EP), an anti-inflammatory agent, protects against the early phase of AILI but impairs late phase liver regeneration and aggravates AILI[46]. These observations suggest the role of KC/macrophages in AILI is complex and may be dependent on the injury phase of AILI. In the late phase of liver regeneration of AILI, KC/macrophages may help to resolve the necrosis by phagocytosis of necrotic cells and promote cell proliferation by secreting pro-regeneration cytokines such as TNF-α[58,60].

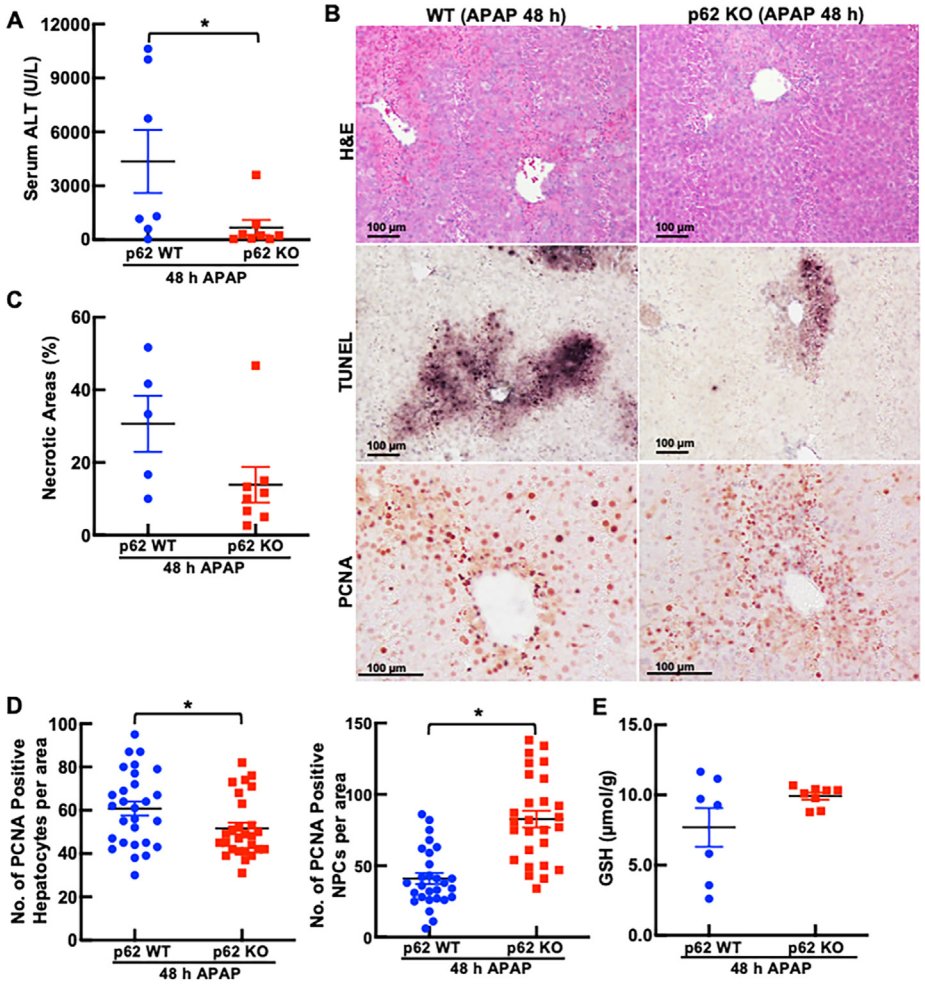

Figure 8 p62 deficiency accelerates liver repair in the late phase of AILI. Male WT and p62 KO mice were treated with APAP (500 mg/kg, i.p.) for 48 h. (A) The levels of serum ALT activities were quantified. Data are presented as mean ± SE ($n \geq 3$). *$P < 0.05$ from Student *t*-test. (B) Representative images of H&E and TUNEL staining in mouse livers (magnification 100×). Representative images of PCNA staining of mouse livers (magnification 200×). (C) Quantification of the necrotic areas from H&E of (B). Each dot represents one mouse, and data are presented as mean ± SE ($n > 3$). *$P < 0.05$ from Student *t*-test. (D) Quantification of the PCNA-positive hepatocytes and PCNA-positive non-parenchymal cells (NPCs) of (B). Data are presented as mean ± SE ($n > 10$). *$P < 0.05$ from Student *t*-test. (E) Total hepatic GSH contents were determined, and data are presented as mean ± SE ($n \geq 3$).

A recently published study reveals that increased hepatic deposition of the platelet-adhesive glycoprotein von Willebrand factor (VWF) contributes to exacerbating AILI[16]. VWF does not involve in the initiation of APAP hepatotoxicity, and overdosing APAP decreases the clearance of VWF, leading to persistent platelet accumulation and delayed repair of AILI[16]. However, complex dual roles of platelets in liver injury have been reported. Platelets accumulation contributes to cholestastic liver injury by promoting leukocyte recruitment and inflammation[61]. In contrast, platelets also promote liver regeneration by releasing HGF, VEGF and insulin-like growth factor 1. Moreover, platelets interact with KC and sinusoidal endothelial cells to stimulate release of IL-6 and VEGF from these cells[62]. A more recent study showed that platelets accumulation worsens the liver recovery in AILI mediated by the platelet receptor CLEC-2 (C-type lectin-like receptor)[63]. APAP overdose increased production of podoplanin, the ligand of CLEC-2, which recruits platelet to the injured liver. Platelet-specific CLEC-2 KO mice had decreased hepatic platelet accumulation and did not show difference of liver injury at early time point (24 h) but significantly improved liver injury at late time points (48−72 h) after APAP overdose. Blocking the CLEC-2/podoplanin axis enhanced neutrophil granulocyte recruitment to the injured liver, which help to phagocytose necrotic cell debris to promote liver recovery during the late phase of AILI. These new findings support a detrimental role of platelets and a beneficial role of neutrophils in the late phase of AILI[57].

The findings in the present study that hepatic VWF and platelet accumulation significantly decreased at 48 h after APAP in p62 KO mice compared with WT mice are well correlated with the improved recovery of AILI in p62 KO mice, which may suggest a detrimental role of VWF and platelet accumulation in the recovery phase of AILI. One intriguing unanswered question is how p62 would affect VWF and platelet recruitment to the liver. VWF is secreted from intracellular Weibel−Palade bodies (WPBs) by endothelial cells, and VWF then recruits platelets to the injured sites on vessel wall[16,64]. It has been reported that autophagy is required for the processing, maturation and secretion of VWF in endothelial cells[64]. Pharmacological inhibition of autophagy or

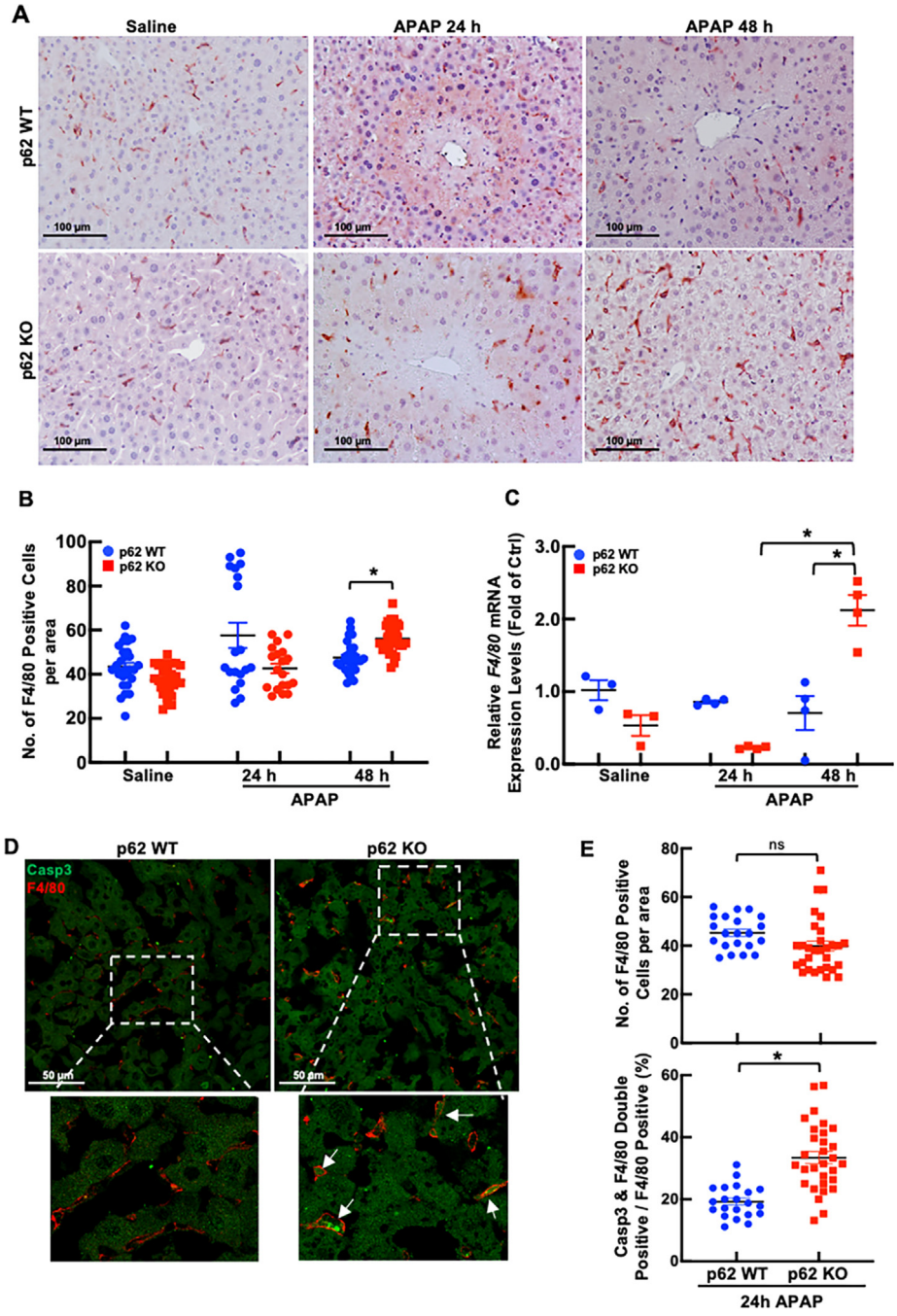

Figure 9 p62 deficiency increases F4/80-positive cells in the late phase of AILI. Male WT and p62 KO mice were treated with APAP (500 mg/kg, i.p.) or saline for 24 or 48 h. (A) Representative images of immunohistochemical staining of F4/80 in mouse livers (magnification 200×). (B) Quantification of the F4/80-positive cells of (A). Data are presented as mean ± SE ($n > 10$). *$P < 0.05$ from one-way ANOVA followed by Dunnett's *post hoc* test. (C) Quantitative real-time PCR analysis of the expression of *F4/80* (*Adgre1*) in mouse livers. Data are presented as mean ± SEM ($n \geq 3$). *$P < 0.05$ from one-way ANOVA followed by Tukey's HSD *post hoc* test. (D) Representative images of hepatic cleaved caspase 3 (Casp3) immunofluorescent labeling (green), and F4/80 (red) (magnification 400×). (E) Quantification of total F4/80 positive cells per image or quantification of F4/80 and Casp3 double positive cells per image of (D). Data are presented as mean ± SE ($n = 21-30$ images from four WT and five p62 KO mice). *$P < 0.05$ from Student *t*-test.

genetic knockdown or deletion of *Atg5* or *Atg7 in vitro* or *in vivo* impaired the secretion of VWF[64]. It remains to be studied whether autophagy receptor proteins such as p62 would be required for secretory autophagic cargo recognition and secretion including VWF. However, no difference of serum VWF levels were detected between WT and P62 KO mice post APAP treatment, suggesting the p62 may not be required for the secretion of VWF in endothelial cells. Secreted VWF eventually are cleared by macrophages and macrophage-specific deficiency of low-density lipoprotein receptor-related protein-1 increases the half-life of

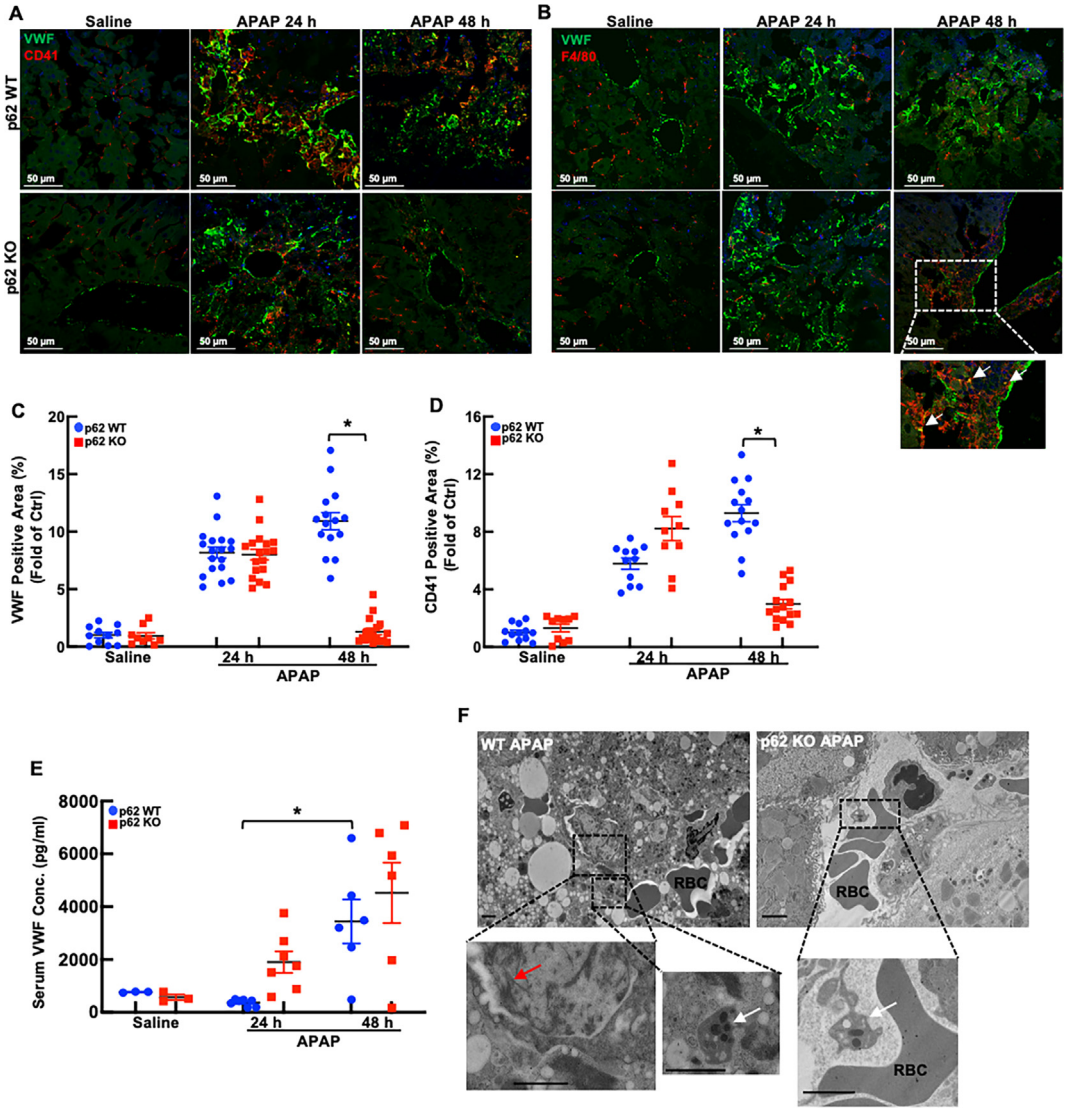

Figure 10 p62 deficiency inhibits VWF deposition and platelet aggregation in the late phase of AILI. Male WT and p62 KO mice were treated with APAP (500 mg/kg, i.p.) or saline for 24 or 48 h. (A) Representative images of hepatic VWF immunofluorescent labeling (green), and CD41 (red) (magnification 400 ×). (B) Representative images of hepatic VWF immunofluorescent labeling (green), and F4/80 (red) (magnification 400 ×). (C, D) Quantification of the VWF-positive area or CD41-positive area of (A). Data are presented as mean ± SE ($n = 10-18$ images from more than 3 mice). *$P < 0.05$ from one-way ANOVA followed by Tukey's HSD *post hoc* test. (E) Serum VWF levels were measured by enzyme-linked immunosorbent assay. *$P < 0.05$ from one-way ANOVA followed by Tukey's HSD *post hoc* test. (F) Representative EM images from WT and p62 KO mouse livers at 48 h after APAP treatment are shown. Red arrow denotes fibrin deposition, white arrow denotes platelets. RBC, red blood cells. Scale bar = 500 nm.

VWF in mice[65]. It is likely increased hepatic numbers of macrophages may also contribute to decreased hepatic VWF at 48 h after APAP treatment in p62 KO mice, as we indeed observed colocalization of VWF in F4/80 positive cells. Nonetheless, the mechanisms of how lack of p62 increases hepatic macrophages and decreases VWF and platelets in the late phase of APAP overdose need to be further studied in the future. Moreover, the role of p62 in NPCs in AILI also needs to be further studied using cell type-specific p62 KO mice.

5. Conclusions

Our data indicate dual roles of p62 in APAP-induced liver injury. p62 inhibits the late injury phase by promoting selective autophagic removal of a subset group of APAP-AD and mitophagy but impairs the recovery phase by enhancing hepatic blood coagulation.

Acknowledgments

This study was supported by fundings U01 AA024733, R37 AA020518, R21 AA027250, R01 DK102142, and R01 AG072895 (USA).

Author contributions

Hui Qian, Qingyun Bai, Xiao Yang, Jephte Y. Akakpo and Hong-Min Ni performed the experiments and analyzed the data. Hong-

Min Ni, Lili Ji, Li Yang and Wen-Xing Ding conceived the study. Wen-Xing Ding supervised the project. Thomas Rülicke and Kurt Zatloukal generated key reagent. Hui Qian and Wen-Xing Ding wrote the manuscript and Hartmut Jaeschke, Thomas Rülicke and Kurt Zatloukal revised the manuscript.

Conflicts of interest

The authors have nothing to declare.

References

1. Mowry JB, Spyker DA, Brooks DE, Zimmerman A, Schauben JL. 2015 annual report of the American Association of Poison Control Centers' National Poison Data System (NPDS): 33rd annual report. *Clin Toxicol (Phila)* 2016;**54**:924−1109.
2. Lee WM. Acetaminophen (APAP) hepatotoxicity—isn't it time for APAP to go away?. *J Hepatol* 2017;**67**:1324−31.
3. Larson AM. Acetaminophen hepatotoxicity. *Clin Liver Dis* 2007;**11**: 525−48.
4. Ostapowicz G, Fontana RJ, Schiødt FV, Larson A, Davern TJ, Han SH, et al. Results of a prospective study of acute liver failure at 17 tertiary care centers in the United States. *Ann Intern Med* 2002;**137**: 947−54.
5. Lee WM. Acetaminophen-related acute liver failure in the United States. *Hepatol Res* 2008;**38**:S3−8.
6. Budnitz DS, Lovegrove MC, Crosby AE. Emergency department visits for overdoses of acetaminophen-containing products. *Am J Prev Med* 2011;**40**:585−92.
7. Heard KJ. Acetylcysteine for acetaminophen poisoning. *N Engl J Med* 2008;**359**:285−92.
8. McGill MR, Sharpe MR, Williams CD, Taha M, Curry SC, Jaeschke H. The mechanism underlying acetaminophen-induced hepatotoxicity in humans and mice involves mitochondrial damage and nuclear DNA fragmentation. *J Clin Invest* 2012;**122**: 1574−83.
9. Hinson JA, Roberts DW, James LP. Mechanisms of acetaminophen-induced liver necrosis. *Handb Exp Pharmacol* 2010;**196**:369−405.
10. Yan M, Huo Y, Yin S, Hu H. Mechanisms of acetaminophen-induced liver injury and its implications for therapeutic interventions. *Redox Biol* 2018;**17**:274−83.
11. Ramachandran A, Jaeschke H. Acetaminophen toxicity: novel insights into mechanisms and future perspectives. *Gene Expr* 2018;**18**: 19−30.
12. Huebener P, Pradere JP, Hernandez C, Gwak GY, Caviglia JM, Mu X, et al. The HMGB1/RAGE axis triggers neutrophil-mediated injury amplification following necrosis. *J Clin Invest* 2015;**125**: 539−50.
13. He Y, Feng D, Li M, Gao Y, Ramirez T, Cao H, et al. Hepatic mitochondrial DNA/Toll-like receptor 9/microRNA-223 forms a negative feedback loop to limit neutrophil overactivation and acetaminophen hepatotoxicity in mice. *Hepatology* 2017;**66**:220−34.
14. Ganey PE, Luyendyk JP, Newport SW, Eagle TM, Maddox JF, Mackman N, et al. Role of the coagulation system in acetaminophen-induced hepatotoxicity in mice. *Hepatology* 2007;**46**:1177−86.
15. Holt MP, Cheng L, Ju C. Identification and characterization of infiltrating macrophages in acetaminophen-induced liver injury. *J Leukoc Biol* 2008;**84**:1410−21.
16. Groeneveld D, Cline-Fedewa H, Baker KS, Williams KJ, Roth RA, Mittermeier K, et al. Von Willebrand factor delays liver repair after acetaminophen-induced acute liver injury in mice. *J Hepatol* 2020;**72**: 146−55.
17. Ni HM, McGill MR, Chao X, Du K, Williams JA, Xie Y, et al. Removal of acetaminophen protein adducts by autophagy protects against acetaminophen-induced liver injury in mice. *J Hepatol* 2016;**65**:354−62.
18. Williams JA, Ni HM, Haynes A, Manley S, Li Y, Jaeschke H, et al. Chronic deletion and acute knockdown of Parkin have differential responses to acetaminophen-induced mitophagy and liver injury in mice. *J Biol Chem* 2015;**290**:10934−46.
19. Wang H, Ni HM, Chao X, Ma X, Rodriguez YA, Chavan H, et al. Double deletion of PINK1 and Parkin impairs hepatic mitophagy and exacerbates acetaminophen-induced liver injury in mice. *Redox Biol* 2019;**22**:101148.
20. Katsuragi Y, Ichimura Y, Komatsu M. Regulation of the Keap1−Nrf2 pathway by p62/SQSTM1. *Curr Opin Toxicol* 2016;**1**:54−61.
21. Manley S, Williams JA, Ding WX. Role of p62/SQSTM1 in liver physiology and pathogenesis. *Exp Biol Med (Maywood)* 2013;**238**: 525−38.
22. Katsuragi Y, Ichimura Y, Komatsu M. p62/SQSTM 1 functions as a signaling hub and an autophagy adaptor. *FEBS J* 2015;**282**:4672−8.
23. Pankiv S, Clausen TH, Lamark T, Brech A, Bruun JA, Outzen H, et al. p62/SQSTM1 binds directly to Atg8/LC3 to facilitate degradation of ubiquitinated protein aggregates by autophagy. *J Biol Chem* 2007;**282**: 24131−45.
24. Komatsu M, Kurokawa H, Waguri S, Taguchi K, Kobayashi A, Ichimura Y, et al. The selective autophagy substrate p62 activates the stress responsive transcription factor Nrf2 through inactivation of Keap1. *Nat Cell Biol* 2010;**12**:213−23.
25. Lau A, Wang XJ, Zhao F, Villeneuve NF, Wu T, Jiang T, et al. A noncanonical mechanism of Nrf2 activation by autophagy deficiency: direct interaction between Keap1 and p62. *Mol Cell Biol* 2010;**30**: 3275−85.
26. Jain A, Lamark T, Sjottem E, Larsen KB, Awuh JA, Overvatn A, et al. p62/SQSTM1 is a target gene for transcription factor NRF2 and creates a positive feedback loop by inducing antioxidant response element-driven gene transcription. *J Biol Chem* 2010;**285**: 22576−91.
27. Reisman SA, Csanaky IL, Aleksunes LM, Klaassen CD. Altered disposition of acetaminophen in Nrf2-null and Keap1-knockdown mice. *Toxicol Sci* 2009;**109**:31−40.
28. Gum SI, Cho MK. Recent updates on acetaminophen hepatotoxicity: the role of Nrf2 in hepatoprotection. *Toxicol Res* 2013;**29**:165−72.
29. Ni HM, Boggess N, McGill MR, Lebofsky M, Borude P, Apte U, et al. Liver-specific loss of Atg5 causes persistent activation of Nrf2 and protects against acetaminophen-induced liver injury. *Toxicol Sci* 2012; **127**:438−50.
30. Sanchez-Martin P, Saito T, Komatsu M. p62/SQSTM1: 'Jack of all trades' in health and cancer. *FEBS J* 2019;**286**:8−23.
31. Moscat J, Karin M, Diaz-Meco MT. p62 in cancer: signaling adaptor beyond autophagy. *Cell* 2016;**167**:606−9.
32. Lahiri P, Schmidt V, Smole C, Kufferath I, Denk H, Strnad P, et al. p62/Sequestosome-1 is indispensable for maturation and stabilization of Mallory-Denk bodies. *PLoS One* 2016;**11**:e0161083.
33. Yang H, Ni HM, Guo F, Ding Y, Shi YH, Lahiri P, et al. Sequestosome 1/p62 protein is associated with autophagic removal of excess hepatic endoplasmic reticulum in mice. *J Biol Chem* 2016;**291**:18663−74.
34. Chao X, Wang S, Zhao K, Li Y, Williams JA, Li T, et al. Impaired TFEB-mediated lysosome biogenesis and autophagy promote chronic ethanol-induced liver injury and steatosis in mice. *Gastroenterology* 2018;**155**:865−879.e12.
35. Jaeschke H. Glutathione disulfide formation and oxidant stress during acetaminophen-induced hepatotoxicity in mice *in vivo*: the protective effect of allopurinol. *J Pharmacol Exp Therapeut* 1990;**255**: 935−41.
36. Akakpo JY, Ramachandran A, Kandel SE, Ni H, Kumer SC, Rumack BH, et al. 4-Methylpyrazole protects against acetaminophen hepatotoxicity in mice and in primary human hepatocytes. *Hum Exp Toxicol* 2018;**37**:1310−22.
37. R-Core-Team. R: a language and environment for statistical computing. Vienna: R Foundation for Statistical Computing; 2020.
38. R Studio-Team. Studio: integrated development for R. RStudio. PBC; 2020.
39. Ichimura Y, Waguri S, Sou YS, Kageyama S, Hasegawa J, Ishimura R, et al. Phosphorylation of p62 activates the Keap1−Nrf2 pathway during selective autophagy. *Mol Cell* 2013;**51**:618−31.

40. Hanawa N, Shinohara M, Saberi B, Gaarde WA, Han D, Kaplowitz N. Role of JNK translocation to mitochondria leading to inhibition of mitochondria bioenergetics in acetaminophen-induced liver injury. *J Biol Chem* 2008;**283**:13565−77.
41. Ding WX, Guo F, Ni HM, Bockus A, Manley S, Stolz DB, et al. Parkin and mitofusins reciprocally regulate mitophagy and mitochondrial spheroid formation. *J Biol Chem* 2012;**287**:42379−88.
42. Ding WX, Yin XM. Mitophagy: mechanisms, pathophysiological roles, and analysis. *Biol Chem* 2012;**393**:547−64.
43. Ding WX, Ni HM, Li M, Liao Y, Chen X, Stolz DB, et al. Nix is critical to two distinct phases of mitophagy, reactive oxygen species-mediated autophagy induction and Parkin−ubiquitin−p62-mediated mitochondrial priming. *J Biol Chem* 2010;**285**:27879−90.
44. Zhong Z, Umemura A, Sanchez-Lopez E, Liang S, Shalapour S, Wong J, et al. NF-kappaB restricts inflammasome activation *via* elimination of damaged mitochondria. *Cell* 2016;**164**:896−910.
45. Ju C, Reilly TP, Bourdi M, Radonovich MF, Brady JN, George JW, et al. Protective role of Kupffer cells in acetaminophen-induced hepatic injury in mice. *Chem Res Toxicol* 2002;**15**:1504−13.
46. Yang R, Zou X, Koskinen ML, Tenhunen J. Ethyl pyruvate reduces liver injury at early phase but impairs regeneration at late phase in acetaminophen overdose. *Crit Care* 2012;**16**:1−9.
47. Miyakawa K, Joshi N, Sullivan BP, Albee R, Brandenberger C, Jaeschke H, et al. Platelets and protease-activated receptor-4 contribute to acetaminophen-induced liver injury in mice. *Blood* 2015;**126**:1835−43.
48. Taniguchi K, Yamachika S, He F, Karin M. p62/SQSTM1-Dr. Jekyll and Mr. Hyde that prevents oxidative stress but promotes liver cancer. *FEBS Lett* 2016;**590**:2375−97.
49. Xie Y, McGill MR, Du K, Dorko K, Kumer SC, Schmitt TM, et al. Mitochondrial protein adducts formation and mitochondrial dysfunction during *N*-acetyl-*m*-aminophenol (AMAP)-induced hepatotoxicity in primary human hepatocytes. *Toxicol Appl Pharmacol* 2015;**289**:213−22.
50. McGill MR, Williams CD, Xie Y, Ramachandran A, Jaeschke H. Acetaminophen-induced liver injury in rats and mice: comparison of protein adducts, mitochondrial dysfunction, and oxidative stress in the mechanism of toxicity. *Toxicol Appl Pharmacol* 2012;**264**:387−94.
51. Chen Y, Liu K, Zhang J, Hai Y, Wang P, Wang H, et al. c-Jun NH_2-terminal protein kinase phosphorylates the Nrf2-ECH homology 6 domain of nuclear factor erythroid 2-related factor 2 and down-regulates cytoprotective genes in acetaminophen-induced liver injury in mice. *Hepatology* 2020;**71**:1787−801.
52. He J, Chen J, Wei X, Leng H, Mu H, Cai P, et al. Mammalian target of rapamycin complex 1 signaling is required for the dedifferentiation from biliary cell to bipotential progenitor cell in zebrafish liver regeneration. *Hepatology* 2019;**70**:2092−106.
53. Ni HM, Bockus A, Boggess N, Jaeschke H, Ding WX. Activation of autophagy protects against acetaminophen-induced hepatotoxicity. *Hepatology* 2012;**55**:222−31.
54. Sun H, Ni HM, McCracken JM, Akakpo JY, Fulte S, McKeen T, et al. Liver-specific deletion of mechanistic target of rapamycin does not protect against acetaminophen-induced liver injury in mice. *Liver Res* 2021;**5**:79−87.
55. Ni HM, Chao X, Yang H, Deng F, Wang S, Bai Q, et al. Dual roles of mammalian target of rapamycin in regulating liver injury and tumorigenesis in autophagy-defective mouse liver. *Hepatology* 2019;**70**:2142−55.
56. Umemura A, Park EJ, Taniguchi K, Lee JH, Shalapour S, Valasek MA, et al. Liver damage, inflammation, and enhanced tumorigenesis after persistent mTORC1 inhibition. *Cell Metabol* 2014;**20**:133−44.
57. Jaeschke H, Ramachandran A. Pleiotropic roles of platelets and neutrophils in cell death and recovery during acetaminophen hepatotoxicity. *Hepatology* 2020;**72**:1873−6.
58. Jaeschke H, Ramachandran A. Mechanisms and pathophysiological significance of sterile inflammation during acetaminophen hepatotoxicity. *Food Chem Toxicol* 2020;**138**:111240.
59. Fisher JE, McKenzie TJ, Lillegard JB, Yu Y, Juskewitch JE, Nedredal GI, et al. Role of Kupffer cells and toll-like receptor 4 in acetaminophen-induced acute liver failure. *J Surg Res* 2013;**180**:147−55.
60. Krenkel O, Mossanen JC, Tacke F. Immune mechanisms in acetaminophen-induced acute liver failure. *Hepatobiliary Surg Nutr* 2014;**3**:331−43.
61. Laschke MW, Dold S, Menger MD, Jeppsson B, Thorlacius H. Platelet-dependent accumulation of leukocytes in sinusoids mediates hepatocellular damage in bile duct ligation-induced cholestasis. *Br J Pharmacol* 2008;**153**:148−56.
62. Chauhan A, Adams DH, Watson SP, Lalor PF. Platelets: no longer bystanders in liver disease. *Hepatology* 2016;**64**:1774−84.
63. Chauhan A, Sheriff L, Hussain MT, Webb GJ, Patten DA, Shepherd EL, et al. The platelet receptor CLEC-2 blocks neutrophil mediated hepatic recovery in acetaminophen induced acute liver failure. *Nat Commun* 2020;**11**:1939.
64. Torisu T, Torisu K, Lee IH, Liu J, Malide D, Combs CA, et al. Autophagy regulates endothelial cell processing, maturation and secretion of von Willebrand factor. *Nat Med* 2013;**19**:1281.
65. Rastegarlari G, Pegon JN, Casari C, Odouard S, Navarrete AM, Saint-Lu N, et al. Macrophage LRP1 contributes to the clearance of von Willebrand factor. *Blood* 2012;**119**:2126−34.